Radiation Interaction with Particulates in Planetary Entry Flows

Andrew Hinkle*, and Serhat Hosder†
Missouri University of Science and Technology, Rolla, MO 65409

Christopher Johnston‡, and Kyle Thompson§
NASA Langley Research Center, Hampton, VA 23681

A hypersonic particle phase solver based on a continuum model is implemented in the NASA HyperSolve CFD code. This solver is used to predict particle phase conditions in dusty Mars entry aerothermodynamic environments. Based on this particle phase flowfield, black-body radiative emission from high temperature dust particles is predicted. This emission is used to simulate the radiative heating to the vehicle surface, due to the particle phase, using a ray-tracing approach. The surface heating due to this particle phase emission is found to be small relative to convective and gas phase radiative heating. In addition to the Mars analysis, the effect of atmospheric haze particulates vaporizing in the Titan atmosphere is studied. The increase in carbon availability due to the composition of the haze particles is found to increase the gas radiative heating. An increase in the radiative heating of up to 3% on the forebody of a representative Titan entry vehicle is predicted with approximately 0.15% haze in the freestream by mass.

Nomenclature

I_ν	=	radiative intensity, W s cm^{-1} sr^{-1}
κ	=	absorption coefficient, cm^{-1}
κ_s	=	scattering coefficient, cm^{-1}
j	=	emission coefficient, W cm^{-3} sr^{-1}
ν	=	frequency, s^{-1}
q	=	radiative flux, W cm^{-2}
$\Phi(\Omega, \Omega')$	=	scattering phase function
Ω	=	view orientation angle, rad
Ω'	=	incident view orientation angle, rad
$d\Omega$	=	solid angle, sr
$\vec{x}$	=	spatial location
z	=	normal distance from a surface, cm
n	=	number density of particles, m^{-3}
ρ	=	density
β	=	freestream particle mass ratio
c_p	=	heat capacity, J kg^{-1} K^{-1}
r	=	radius, m
ϵ	=	emissivity
Subscripts		
∞	=	freestream value
p	=	particle quantity
g	=	gas quantity
ν	=	frequency varying property

*Graduate Student, Department of Mechanical and Aerospace Engineering
†Professor of Aerospace Engineering, Department of Mechanical and Aerospace Engineering, AIAA Associate Fellow
‡Aerospace Engineer, Aerothermodynamics Branch, Research Directorate, AIAA Associate Fellow
§Aerospace Engineer, Aerothermodynamics Branch, Research Directorate

I. Introduction

The presence of dust in hypersonic flight and planetary entry pose numerous challenges for vehicle design. In the case of a Mars entry, global dust storms result in dust loading sufficient to significantly increase surface recession via particulate impact [1, 2]. Particulates can also affect the aerothermodynamic environment of the vehicle by altering the shock-layer characteristics [3, 4]. The coupling of mass, momentum, and energy between the gas and particulate phases can result in increased convective heating to the surface by increasing the total enthalpy of the pure gas flow. For radiating gas environments, however, additional interaction mechanisms between the gas and particulate arise via scattering, emission, and absorption. Particulates that vaporize in shock-layers can additionally introduce new species to the flow that can have relatively strong emission characteristics. As multiple planetary mission targets have atmospheres with particulate presence, it is important to characterize these effects and determine the sensitivity of surface heating predictions to these mechanisms.

In recent years, there has been increasing interest in studying mixed phase hypersonic gas-particle flows, building upon works that employed simplified models and scenarios in hypersonic flight problems [5, 6]. These works were focused mostly on particulates like ice crystals and rain water for high-speed vehicles in Earth's atmosphere, but were the foundation built upon by many later studies investigating the effect of Mars dust on entry vehicles [7, 8]. Early papers studying the effect of Mars dust on entry conditions focused mostly on the impact it had on erosion of the thermal protection system material, utilizing more basic descriptions of the Martian atmospheric dust loading [7, 8]. These works, despite their limited scope and modeling, established that erosion effects are more significant for aerocapture missions. It was also shown that the way in which the dust size and dust mass loading are modeled can have a significant impact on the predicted erosion augmentation. More recently, Palmer et al. [1] utilized improved modeling of Mars atmospheric dust loading, analyzing both dust and thermochemical erosion of a vehicle TPS over an entire planetary entry trajectory. Following these works, Hinkle et al. [2] presented an efficient method for solving surface erosion problems over arbitrary vehicle geometries, as well as an uncertainty quantification and sensitivity analysis study, which identified the characterization of atmospheric dust material and size distributions to be the most important sources of uncertainty. Recent papers have further sought to study the effects of coupling between the dissimilar phases, and have shown the presence of particles near the vehicle can augment the convective heat flux [3, 4, 9]. These works were mostly concerned with convective heating, and didn't study the impact of the particulate fields on radiative transport. Some work has occurred in this area [10] for solid rocket plume particulates, but less has been seen for planetary entry problems.

The objective of this paper is to model and investigate the effect of atmospheric particulates on the radiative heating of planetary entry vehicles. A solid particle phase solver based on a continuum model is detailed and demonstrated on a model problem relevant to Mars entry. The solver is used to compute the number density and state of dust particles through the gas domain, which is used to estimate the black-body radiative emission due to high temperature particles. The black-body emission is integrated to the surface using a ray tracing approach to determine the amount of radiative heat flux to the vehicle, which may arise due to the surrounding shock-heated particles. Additionally, a preliminary analysis of the effect of atmospheric haze particulate vaporization products on radiative heat flux in Titan entry is presented.

II. Solution Methodology

This section describes the Eulerian-Eulerian multiphase solution approach utilized, which is based on a computational fluid dynamics (CFD) solver and continuum solid particle phase model. A description of the solid phase governing equations and solution methodologies is presented. Next, a brief overview of the radiative transport equation and angular integration techniques used in this study is given, including discussion of the modeling of specific mechanisms like black-body emission.

A. Description of Gas and Particle Solvers

In this work, the gas phase was solved using the NASA HyperSolve CFD code, developed at the NASA Langley Research Center. HyperSolve is a node-centered, edge-based discretization utilizing a compact 3^{rd}-order upwind finite volume scheme [11], which has been developed for use in aerothermodynamics problems in which accurate surface gradients on simplex meshes can be recovered for the prediction of heat flux. Refine, an unstructured mesh adaptation tool based on solution interpolation error estimates [12], was used to adapt an initial tetrahedral mesh based on a given

metric field using the Sketch-to-Solution workflow [13]. In this study, the mesh adaptation metric was constructed using the Hessian of the density solution predicted by HyperSolve. The solution was advanced to steady state using a Jacobian free Newton-Krylov (JFNK) solver [14].

Planetary entry scenarios typically involve particle mass loadings levels which are quite small ($\beta \ll 1$), therefore, the solid particle phase was assumed to be dilute and have no interparticle collisions. Under these assumptions, as well as the steady gas flow assumption, the particle trajectories and thermal state are only influenced by the effect of the surrounding gas. As particles are on the micron scale, and much smaller than the characteristic length scale of a planetary entry problem, a Lagrangian point mass assumption is suitable. Under this assumption, each particle being solved is treated as a point mass with a state vector consisting of its position (x_p, y_p, z_p), velocity (u_p, v_p, w_p), and temperature (T_p):

$$\mathbf{U}^T = \begin{bmatrix} x_p & y_p & z_p & u_p & v_p & w_p & T_p \end{bmatrix}, \tag{1}$$

and the time derivative of this state vector is the set of governing equations for the particle:

$$\frac{d\mathbf{U}}{dt} = \begin{bmatrix} u_p \\ v_p \\ w_p \\ \frac{3\rho_g C_D}{8\rho_p r_p} \left\|\Delta\vec{v}\right\| u_p \\ \frac{3\rho_g C_D}{8\rho_p r_p} \left\|\Delta\vec{v}\right\| v_p \\ \frac{3\rho_g C_D}{8\rho_p r_p} \left\|\Delta\vec{v}\right\| w_p \\ \frac{3\kappa_g Nu}{2\rho_p c_{P_p} r_p^2} \left(T_g - T_p\right) \end{bmatrix}. \tag{2}$$

Various approaches for estimating quantities such as number density using a Lagrangian model have been used in hypersonic problems, [2–4, 15]. Depending on the problem, these approaches can vary in complexity or computational cost. For example, if the vehicle wake is to be considered, the cost and complexity issues of Lagrangian methods are exaggerated due to the large difference in length scales and particle trajectories through the domain. Instead, a continuum model for the solid particle phase was used for the current work as this allows the number density of the solid phase to be computed using the same techniques as the gas phase solution. The continuum model is formed by considering a stationary control volume and integrating the flux of mass, momentum, and energy carried by the solid phase across the control volume boundaries. This model, which has found use in numerous studies in the aerospace literature [9, 16–18], takes the following form:

$$\frac{d}{dt}\mathbf{U}_p = \nabla \cdot \mathbf{F}\left(\mathbf{U}_p\right) = \mathbf{S}_p, \tag{3}$$

where $\mathbf{U}_p$ is the particle phase state vector, $\mathbf{F}\left(\mathbf{U}_p\right)$ is the particle phase flux vector, and $\mathbf{S}_p$ is the source vector. The state vector for the particle phase takes the following form:

$$\mathbf{U}_p = \begin{bmatrix} \rho_p \\ \rho_p \vec{u}_p \\ \rho_p E_p \end{bmatrix}, \tag{4}$$

where ρ_p, $\vec{u}_p$, and E_p are the mass density, velocity vector, and total energy per unit mass of the particle phase, respectively. The mass density can be expressed as the product of the number density, n_p, of particles at a point in space and the mass of the particles, m_p:

$$\rho_p = n_p m_p. \tag{5}$$

A distribution of particle sizes can be modeled by integrating an output quantity weighted by a mass fraction function as discussed in Ref. [2]. The resulting flux function is:

$$\mathbf{F}\left(\mathbf{U}_p\right) = \begin{bmatrix} \rho_p \vec{u}_p \\ \rho_p \vec{u}_p \vec{u}_p \\ \rho_p \vec{u}_p E_p \end{bmatrix}. \tag{6}$$

Lastly, the source vector is:

$$\mathbf{S}_p = \begin{bmatrix} 0 \\ \vec{F}_p \\ \dot{Q}_p + \vec{u}_p \cdot \vec{F}_p \end{bmatrix}, \tag{7}$$

where $\vec{F}_p$, and $\dot{Q}_p$ are the volumetric force and heat transfer from the gas phase to the particle phase. Assuming spherical particles, $\vec{F}_p$ can be expressed as follows:

$$\vec{F}_p = \frac{3}{8}\frac{\rho_p \rho_g}{r_p \rho_m} C_D \left\| \Delta\vec{v} \right\| \left(\vec{u}_g - \vec{u}_p \right), \tag{8}$$

where C_D is the drag coefficient. For the current study, the model of Loth et al. [19] was used for the particulate drag coefficient. The volumetric heat transfer can be expressed as follows:

$$\dot{Q}_p = \frac{3}{2}\frac{\rho_p \kappa_g \mathrm{Nu}}{\rho_m r_p^2} \left(T_g - T_p \right) - \frac{3\rho_p \epsilon \sigma T_p^4}{\rho_m r_p}, \tag{9}$$

where Nu is the Nusselt number. For the current study, the model of Fox et al. [20] was used for the particle Nusselt number.

The system in Eq. (3) is essentially the Euler equations with no contribution of a pressure term to the flux, and a source term vector imposing the effect of an accompanying gas phase solution on the particle phase state. As Eq. (3) shares such similarity to the inviscid compressible gas phase equations, the solution techniques were shared between the phases. Due to the similarities in modeling, the particle phase solver was added to the existing gas phase solver in HyperSolve. The particle solver functionality was implemented through three additions. The first addition was that of a flux function for the system. The flux function was implemented as a Steger-Warming flux vector splitting[21]:

$$F(\mathbf{U}) = F^+ + F^-, \tag{10}$$

where $F^\pm$ are the splittings of $\mathbf{F}\left(\mathbf{U}_p\right)$ on each side of an interface. $F^\pm$ is expressed as follows:

$$F^\pm = u_p^\perp \begin{bmatrix} \rho_p \\ \rho_p \vec{u}_p \\ \rho_p E_p \end{bmatrix}, \tag{11}$$

where $u_p^\perp$ is the velocity normal to the cell interface. However, using this flux function directly results in numerical instability. Some approaches use a pseudopressure term so that more advanced flux functions can be utilized without modification [17]. We instead chose to add a simple dissipation term to stabilize the convective flux:

$$F(\mathbf{U}_p) = F^+ + F^- + \frac{A_F}{2} e_{\max} \left(U^+ - U^- \right), \tag{12}$$

where A_f is the cell interface area, and $e_{\max}$ is the maximum eigenvalue of the system at the interface. The maximum eigenvalue of the system at the interface is simply the maximum of the interface normal velocity on each each side of the interface. A limiter was added that prevents the maximum eigenvalue from falling below a specified value, which was taken to be a nondimensional speed of 0.1 in this study.

The second addition made to HyperSolve was the evaluation of the source vector given in Eq. (7). The gas phase solution state was used to determine the values in the source term. The last addition, which enabled the modeling of a solid particle phase using a continuum model, was that of a shadowing boundary condition. In this work, the particles did not rebound from solid vehicle surfaces. Similar to Refs. [1, 2], particles are assumed to embed into the thermal protection system (TPS) of an entry vehicle. An extrapolation boundary condition can be used to model the assumption that particles leave the domain unaffected by solid surfaces. This boundary condition is incorrect for the wake of a vehicle, however, where the particle number density is zero due to the inability of particles to perfectly follow gas streamlines and recirculate into the wake. Jung and Myong [17] present a shadowing boundary condition that switches between extrapolation and a zero-valued Dirichlet boundary condition depending on the directionality of particles with

respect to the wall. For particle velocities pointing into the wall, extrapolation is used, while a zero-valued Dirichlet condition is used otherwise. In the current work, only the density was set to zero for shadowed walls. The boundary was implemented as follows:

$$\begin{aligned} U_{\text{wall}} &= U_{\text{interior}}, \\ \rho_{\text{wall}} &= 0 \text{ if } \vec{u}_p \cdot \hat{n} \leq 0. \end{aligned} \tag{13}$$

While both the gas and particle phase solutions are coupled, the effect of the particle phase on the gas phase flow is negligible for conditions representative of most planetary entry problems [2, 15]. Therefore, two-way coupling was neglected in this work.

B. Radiation Transfer

Radiative transfer is modeled using a ray analogy, in which the steady-state radiant intensity for a given wavelength along a line of sight is gained or lost due to the effects of absorption, emission, and scattering through the medium [22, 23]. Radiative flux to a surface is then computed by casting rays in many directions and integrating the incident intensity over the field of visibility of the point:

$$q(\vec{x}) = \int_0^{\infty} \int_0^{2\pi} \int_0^{\pi/2} I_\nu(\vec{x}, \phi, \theta) cos(\phi) sin(\phi) d\phi d\theta d\nu, \tag{14}$$

where the subscript ν refers to the wavelength of the radiation. Under this ray analogy, the intensity along a line of sight is governed by the radiative transfer equation (RTE), which is an integrodifferential equation that describes the intensity change along a line of sight [24]:

$$\underbrace{\frac{\partial}{\partial s}\left[I_\nu(s,\Omega)\right]}_{\text{(i)}} + \underbrace{\left\{\kappa_\nu(s) + \kappa_{\nu(s),s}\right\} I_\nu(s,\Omega)}_{\text{(ii)}} = \underbrace{j_\nu(s) I_\nu(s,\Omega)}_{\text{(iii)}} + \underbrace{\frac{\sigma_\nu(s)}{4\pi} \int_{4\pi} I_\nu(s,\Omega') \Phi(s,\Omega,\Omega') d\Omega'}_{\text{(iv)}}. \tag{15}$$

The four terms of the RTE represent (left-to-right) the (i) change in radiative intensity along a ray, (ii) losses due to absorption and out-scattering, (iii) gains due to emission, and (iv) gains due to in-scattering. In the current study, the absorption and scattering mechanisms were neglected for simplicity, which can also be interpreted as the limiting case for surface radiative heating augmentation due to particles considering only the emission from the particles. Inclusion of the effects of scattering and absorption are the subject of ongoing study.

1. Radiative Emission due to High Temperature Particles

High temperature particulates emit black-body radiation, which is a function of their surface temperature. In the current study, this emission mechanism is modeled with no detailed wavelength dependence due to the neglected gas absorption. The black-body emissive flux from a surface with emissivity ϵ and temperature T, once integrated over all wavelengths, is as follows:

$$q_{\mathbf{b}} = \epsilon \sigma T^4, \tag{16}$$

where σ is the Stefan-Boltzmann constant. For a particle cloud, the total amount of energy radiated from a constant radius particle phase in a unit volume is the product of the number density, n_p, the surface area of a particle, $A_{\text{s,p}}$, and Eq. (16):

$$\dot{Q}_{\text{rad,p}} = n_p A_{\text{s,p}} \epsilon \sigma T_p^4. \tag{17}$$

Assuming spherical particles of radius, r_p, and substituting Eq. (5) for the number density, the following expression for the volumetric radiative energy exchange from the particle phase is obtained:

$$\dot{Q}_{\text{rad,p}} = \frac{3 \rho_p \epsilon \sigma T_p^4}{\rho_m r_p}. \tag{18}$$

The emission coefficient, which is the amount of energy radiated from a unit volume over a differential solid element, $d\Omega$, is computed by assuming isotropic emission. For isotropic emission, the volumetric radiation power is divided by the total spherical solid angle, which is 4π:

$$j_{\mathrm{b,p}} = \frac{3\rho_p \epsilon \sigma T_p^4}{4\pi \rho_m r_p}. \tag{19}$$

The emission coefficient in Eq. (19) was used to evaluate the emission term in Eq. (15), which was integrated numerically using the trapezoidal rule.

2. Ray Traced Radiation Flux Integration

In the current study, the radiative heat flux to a surface given in Eq. (14) was computed using a ray-tracing approach. In the ray-tracing approach, discrete rays are cast out from a point to compute the radiative intensity arriving at the location from the direction of the ray [22]. In the current study, Eq. (14) was discretized over the hemisphere of visibility at a surface point according to Refs. [22, 23]. Assuming zero intensity at the farthest point on each ray, the RTE was integrated toward the surface to compute the intensity at the wall for the incoming ray direction. These wall intensity values are then integrated over the solid angle to compute the flux. One important consideration for vehicles, that have concavity to their surface geometry, was to clip rays which contact other points on the vehicle surface. In the current study, rays were tested for intersection with the solid surface facets to determine the minimum intersection distance. If an intersection was detected, the ray maximum trace distance was set to the minimum wall intersection distance. An example of ray clipping is shown in Fig. 1, where the rays that 'see' the second biconic region of the MSL backshell [25] are clipped at the surface, rather than being able to pass through to the forebody region.

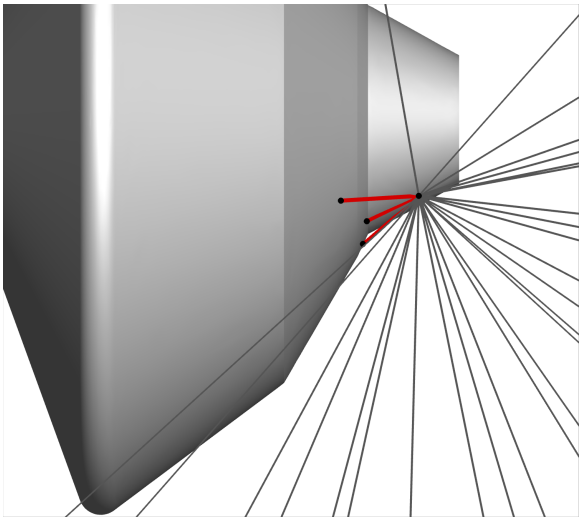

Fig. 1 Rays cast from a surface location, which have visibility of other surface points.

III. Results and Discussion

A. Radiative Heating due to Shock-Heated Particles in Mars Entry

In Mars EDL during global dust storm conditions, dust particulate loading in the atmosphere can pose a significant risk of thermal protection system (TPS) erosion [1, 2]. Dust particles, which pass through the shock-layer around a vehicle, can become heated by high temperatures and a secondary shock-layer in front of the particle. At high temperatures, particles can begin to radiate strongly. In this study, the total radiative emission from the shock-heated dust particle phase was considered as a potential heating mechanism for vehicles entering Mars during a dust storm condition. The local emission from the dust particles was considered with no wavelength dependence, and the absorption of radiation by the gas phase was assumed negligible. Assuming no gas absorption results in an overprediction of the heat flux by the particle phase.

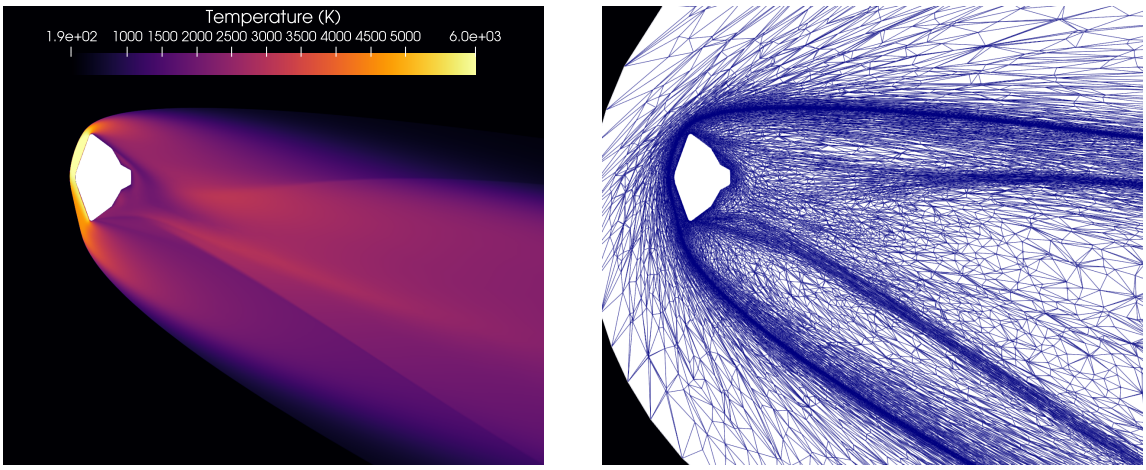

(a) Temperature field. **(b) Adapted mesh.**

Fig. 2 Gas phase solution for the conditions given in Table 1.

For the current work, a representative condition and vehicle geometry relevant to the MSL [25] and Mars2020 [26] missions was chosen as a case study. A condition representative of a 20 km altitude trajectory point was considered, as shown in Table 1. This condition, which is representative of a later point in the trajectory, had a Mach number of

Table 1 Freestream conditions for Mars entry case study.

V_∞ (m s^{-1})	T_∞ (K)	ρ_∞ (kg m$^-3$)	α (deg.)
3200	188	2.6×10^{-3}	-16.8

approximately 14. While dissociation still occurs at this condition, a perfect gas assumption was made for simplicity. The solution was performed in HyperSolve by beginning with a coarse tetrahedral mesh of approximately 200,000 nodes, and adapting to the density solution using Refine as discussed in Sec. II.A up to approximately 500,000 nodes over 6 adaptation cycles. The resulting gas temperature solution and mesh is shown in Fig. 2.

The particle phase was treated with the continuum approach detailed in Sec. II.A, assuming a constant particle radius for simplicity. The conditions of the particle phase are given in Table 2. The velocity, temperature, and angle of attack are the same as the gas solution in the freestream. The dust loading, β_∞, represents a high estimate of dust loading in global storm conditions [1]. The particle radius considered was based on a mass-averaged radius considering the full particle distribution [1, 2, 4]. Figure 3 shows the density ratio and temperature fields of the dust phase predicted using the current methodology. As seen in Fig. 3a, the density rises near the forebody heat shield due to particles slowing down under drag. Some particles, which are slowed but do not contact the vehicle, are transported around the shoulder, resulting in regions of higher density. Behind the vehicle, a 'shadow' formed due to the solid surface boundary condition discussed in Sec. II.A. This 'shadow' region formed where no particles were able to enter due to their inertia. In Fig. 3b, the associated particle temperature field for the particle phase is shown. Despite a shadow region forming, the temperature was defined in the shadow. It is important to note that continuum models differs from Lagrangian models in that a solution is still present for quantities like temperature and velocity in regions with no particles, such as in the 'shadowed' wake region. As quantities such as radiative emission are a function of number density, the temperature in the shadow region did not impact the solution as no particle density was present.

Table 2 Dust phase conditions for Mars entry case study.

β_∞	r_p (μm)	ρ_m (kg m^{-3})	cp_p, (J kg^{-1} K^{-1})	ϵ
0.0001	2.0	2940.0 [1]	700.0 [1]	0.85 [27]

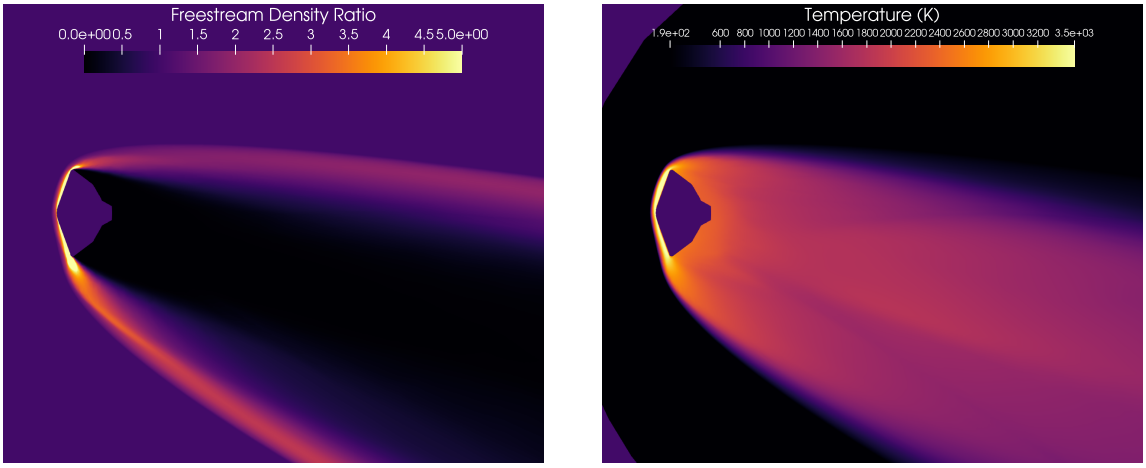

(a) Density ratio field. **(b) Temperature field.**

Fig. 3 Particle phase solution for the conditions given in Table 2.

The radiative emission coefficient, j_b, given in Eq. (19), was evaluated using the density and temperature fields shown in Fig. 3. The emission coefficient, shown in Fig. 4, is the total volumetric energy emitted from the particle phase per unit steradian of solid angle.

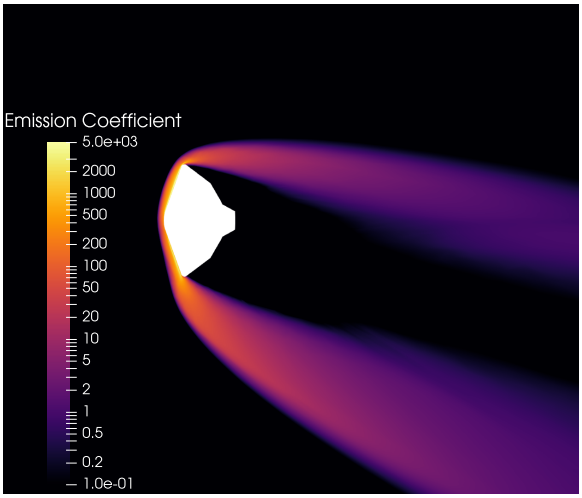

Fig. 4 Emission coefficient resulting from particle black-body radiation for the Mars entry case.

In Fig. 4, due to the strong dependence on the temperature of the particles, significantly higher emission was present in the forebody shock layer region. As the particles passed by the vehicle, they cooled and began to radiate less strongly, causing a fast drop off of emission in the regions just past the shoulder. Using the ray tracing integration technique described in Sec. II.B.2, the heating to the surface was computed. A total of 5 polar angles and 10 equatorial azimuthal points were used, for a total of 29 uniformly distributed rays sampled at each surface location. The surface heating is shown over the full vehicle in Fig. 5 and along the symmetry plane of the vehicle in Fig. 6. The features of the radiative heating, particularly to the backshell from particle black-body emission, are quite similar to gas phase radiation in which the surface geometry can significantly affect the heating due to visibility of the forebody flow [28, 29]. For the condition considered, the heating due to particle black body emission was approximately an order of magnitude smaller than gas phase radiation, and unlikely to impact missions directly [28]. It is important to note the linear dependence on particle density in Eq. (19). As discussed in Ref. [1], dust loading estimates at lower altitudes have significant uncertainty as values must be extrapolated from higher altitudes using the Conrath equation. The uncertainty in surface heating by black-body radiation from particles will be proportional to dust loading uncertainties.

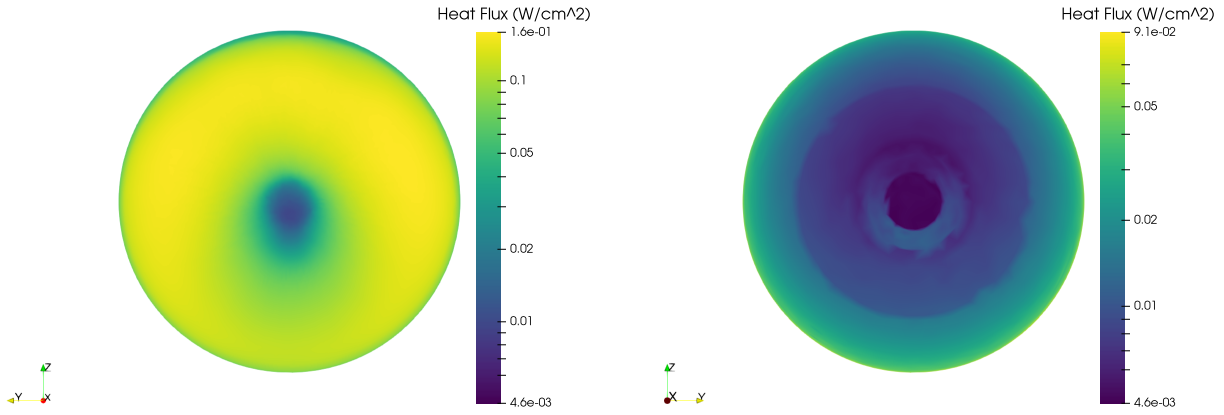

(a) Forebody. **(b) Backshell.**

Fig. 5 Surface radiative heat flux from particle black-body emission for the Mars entry case.

B. Haze Particulate Vaporization Effects in Titan Entry

In recent years, Titan has been a destination of interest for scientific missions, and analysis of entry into the Titan atmosphere has been more common [29]. Similar to Mars and other planetary bodies in the solar system, the Titan atmosphere contains particulates at high altitudes. In the case of Titan, atmospheric haze particles are composed of agglomerated organic monomers [30]. The haze particles form high in the atmosphere and increase in size as they fall toward the surface of Titan [30]. To determine the relationship between the atmospheric density and the haze quantity through the atmosphere, the ratio of haze density to gas density was computed using the haze model of Ref. [30]. The haze density was computed by assuming spherical particles with a density of 1000 kg/m^3 [30] and computing their mass based on the effective spherical radius profile given in Ref. [30]. Multiplying the mass and number density profile of the haze, and dividing by the density of the gas phase results in the haze particle loading. Using the nominal density profile given in Ref. [31], the haze mass loading was computed. Figure 7 shows the mass loading of Haze in Titan's atmosphere as a function of altitude. Through much of the atmosphere, the haze loading ratio was found to be quite small (β « 1%), with the exception of a spike of nearly 0.147% at 460 km. As the haze particulates contain between 76 and 92% carbon, a comparison against the amount of methane present showed an increase of approximately 10% added carbon in the freestream. Since the haze particles at this atltitude have an equivalent spherical radius of approximtaely 0.4 μm [30], it is likely that the particles will heat up fast enough to vaporize within the shock-layer and increase the amount of carbon present for the formation of strong radiating species [29]. Detailed vaporization modeling for the haze particles is the subject of ongoing study.

For this case study, a representative Titan entry vehicle was considered, using conditions representative of a 460 km altitude trajectory point at 7.36 km/s [29]. To study the effect that haze particle vaporization may have on radiative heating, the gas phase was modeled using the NASA LAURA CFD code developed at the NASA Langley Research Center [32]. The atmosphere was modeled with a two-temperature thermochemical nonequilibrium gas model consisting of the following species: N, C, H, N_2, CH_4, CH_3, CH_2, CH, H_2, C_2, NH, CN, HCN, CN^+, H^+, N^+, N_2^+, C^+, and e^- [29]. As a preliminary analysis, the haze particles were assumed to fully vaporize due to their small size and the high heating the particles experience in the shock layer. Under this assumption, the freestream density and mass fractions were changed to account for the elemental composition of the fully vaporized haze particulates. The freestream conditions for the nominal and vaporized haze conditions are given in Table 3, where c_i represents the mass fraction of species i imposed in the freestream. The radiation from the gas phase was computed with the HARA radiation code using a tangent slab model [33].

Figure 8 shows the translational temperature field for the nominal case, and Fig. 9 shows the comparison between nominal and haze vaporization radiative heat flux along the symmetry plane of a representative Titan entry vehicle. As seen in Fig. 9b, near the forebody shoulder an increase of nearly 3% is observed for the haze vaporization case, which is

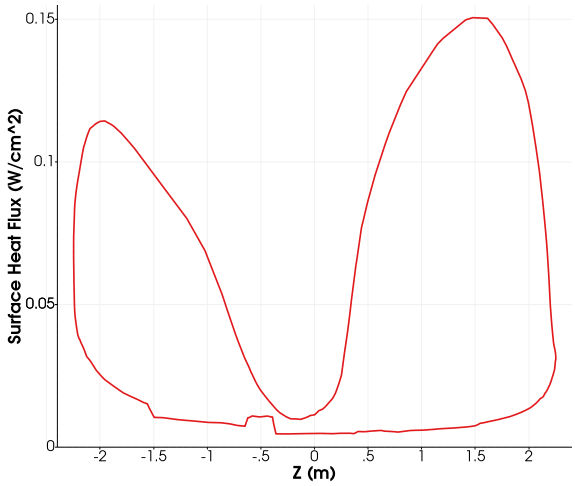

Fig. 6 Surface radiative heat flux along the symmetry plane of the vehicle for the Mars entry case.

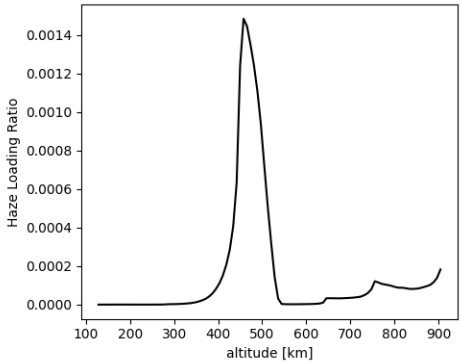

Fig. 7 Haze mass loading ratio for Titan as a function of altitude.

large relative to the quantity of haze in the atmosphere by mass. Overall, the magnitude of the heating increase is unlikely to be a significant factor for mission design in Titan entry scenarios, but a more thorough study with ray-traced radiation, detailed particulate vaporization modeling, and uncertainty in the haze quantity considered would be warranted to understand the effect on the radiation increase.

IV. Conclusions

In this study, a continuum model for solid particle transport in hypersonic flows was implemented in HyperSolve. The particle solver was implemented using a special pressureless flux function and dissipation term. A modified extrapolation boundary condition, which admits regions of zero density in the particle field, was used to model the shadowed wake region behind a vehicle. A ray-tracing radiative transport solver was used to integrate the black-body emission from shock-heated particles over a vehicle surface. Two case studies relevant to planetary entry missions in particle-laden atmospheres were presented. The fist case study considered was a Mars entry scenario during a global dust storm. The effect of the shock layer on the particle density and temperature was presented, and a conservative estimate of the black-body emission through the gas domain was made by neglecting gas absorption. The surface heating by this mechanism was found to be small, with forebody heating on the order of 0.1 W/cm^2, while the backshell heating was much smaller. The second case study considered was a Titan entry scenario. An analysis of the carbon content in the atmospheric haze found that a region of the atmosphere exists in which a large amount of carbon is present relative to the freestream methane content. Assuming the haze to fully vaporize, a comparison was made between a nominal condition and an altered condition in which freestream mass fractions according to the elemental composition of the

Table 3 Conditions for the Titan case.

Case	V_∞ (m s^{-1})	ρ_∞ (kg m^{-3})	T_∞ (K)	c_{N_2}	c_{CH_4}	c_C	c_H	c_N
Nominal	7362.46	8.4700×10^{-6}	165.93	0.9873	0.01270	0	0	0
Vaporized Haze	7362.46	8.4824×10^{-6}	165.93	0.9859	0.01268	1.233×10^{-3}	1.035×10^{-4}	1.307×10^{-4}

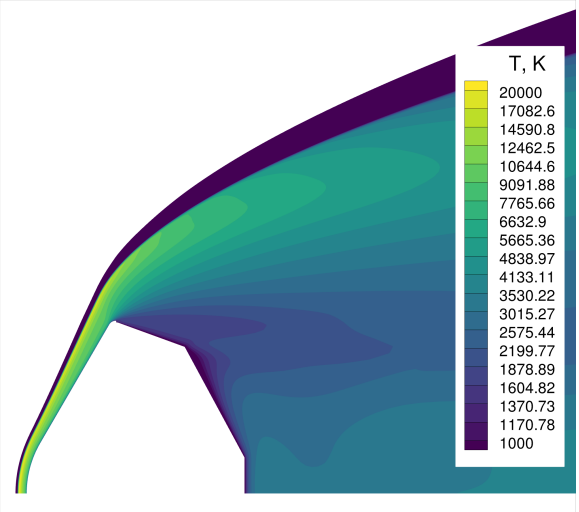

Fig. 8 Translational temperature field for the nominal Titan 460 km case.

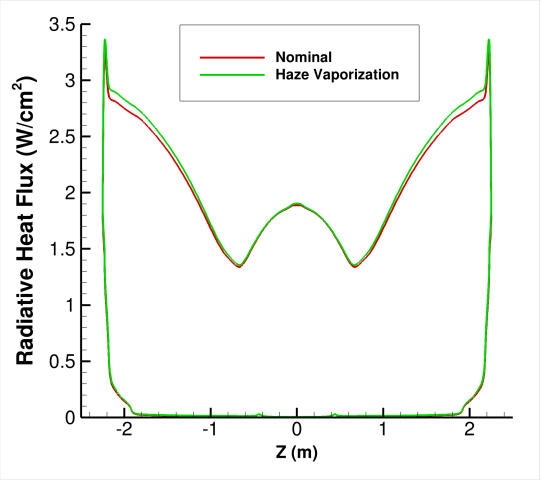

(a) Radiative heat flux.

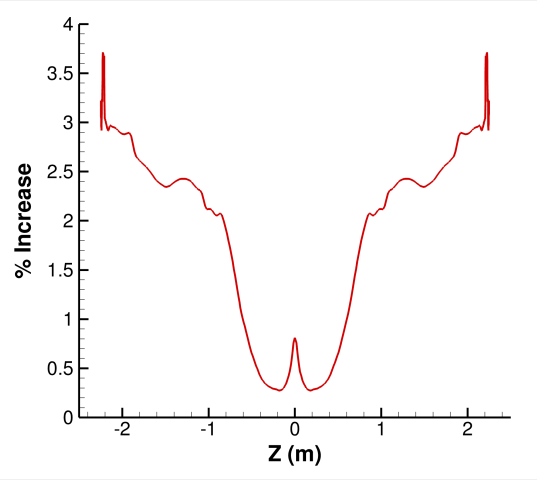

(b) Increase due to haze.

Fig. 9 Comparison of symmetry plane radiative heatinge (a) with and without haze vaporization and (b) percentage increase.

haze. The increase in carbon availability due to the composition of the haze particles was found to increase the gas radiative heating to the vehicle by up to 3% on the forebody of a representative Titan entry vehicle with approximately 0.15% haze in the freestream by mass. The work in progress includes the incorporation of the effects of scattering by particulates on radiative heating as well as detailed mass transfer modeling due to vaporization.

Acknowledgments

This work was supported by a NASA Space Technology Research Fellowship (NSTRF) under grant No. 80NSSC19K1150 (Andrew Hinkle, NSTRF student, Serhat Hosder, principal investigator, and Christopher O. Johnston, research collaborator).

References

[1] Palmer, G., Ching, E., Matthias, I., D., A., and Gulhan, A., "Modeling Heat-Shield Erosion due to Dust Particle Impacts for Martian Entries," *Journal of Spacecraft and Rockets*, Vol. 57, No. 5, 2020, pp. 857–875.

[2] Hinkle, A., Hosder, S., and Johnston, C., "Efficient Solution of Surface Erosion in Particle-Laden Hypersonic Flows," *Journal of Spacecraft and Rockets*, Vol. 59, No. 6, 2022, pp. 2114–2128. https://doi.org/10.2514/1.A35331.

[3] Ching, E., Brill, S., Barnhardt, M., and Ihme, M., "A two-way coupled Euler-Lagrange method for simulating multiphase flows with discontinuous Galerkin schemes on arbitrary curved elements," *Journal of Computational Physics*, Vol. 405, 2020.

[4] Hinkle, A., Hosder, S., and Johnston, C., "Efficient Two-Way Coupled Analysis of Steady-State Particle-Laden Hypersonic Flows," *AIAA Aviation*, Chicago, IL, 2022.

[5] Waldmann, G., and Reinecke, W., "Particle Trajectories, Heating, and Breakup in Hypersonic Shock Layers," *AIAA Journal*, Vol. 9, No. 6, 1971, pp. 1040–1048.

[6] Lin, T., and Thyson, N., "Ice-Crystal/Shock-Layer Interaction in Hypersonic Flight," *AIAA Journal*, Vol. 15, No. 10, 1977, pp. 1511–1514.

[7] Papadopoulos, P., Tauber, M., and Chang, I., "Heatshield Erosion in a Dusty Martian Atmosphere," *Journal of Spacecraft and Rockets*, Vol. 30, No. 2, 1993, pp. 140–151.

[8] Palmer, G., Y.K., C., Papadopoulos, P., and Tauber, M., "Reassessment of Effect of Dust Erosion on Heatshield of Mars Entry Vehicle," *Journal of Spacecraft and Rockets*, Vol. 37, No. 6, 2000, pp. 747–752.

[9] Padmapriya, R., and Reddy, K., "Numerical Analysis of Dusty Hypersonic Viscous Gas Flow over a Flat Plate," *AIAA Journal*, Vol. 39, No. 7, 2001, pp. 1313–1319.

[10] Dombrovsky, L., Reviznikov, D., and Sposobin, A., "Radiative Heat Transfer from Supersonic Flow with Suspended Particles to a Blunt Body," *International Journal of Heat and Mass Transfer*, Vol. 93, 2016, pp. 853–861.

[11] Thompson, N. H., K., and Padway, E., "Economical Third-Order Methods for Accurate Surface Heating Predictions on Simplex Element Meshes," *AIAA SciTech Forum*, National Harbor, MD, 2023.

[12] Park, M. A., "Anisotropic Output-Based Adaptation with Tetrahedral Cut Cells for Compressible Flows," Ph.D. thesis, Massachusetts Institute of Technology, Sep. 2008. https://doi.org/1721.1/46363.

[13] Kleb, W., Park, M., Wood, W., Bibb, K., Thompson, K., and Gomez, R., "Sketch-to-Solution: An Exploration of Viscous CFD with Automatic Grids," *AIAA Aviation*, Dallas, TX, 2019.

[14] Thompson, K., and O'Connell, M., "Streamlined Convergence Acceleration for CFD Codes," *AIAA Aviation*, Dallas, TX, 2019.

[15] Sahai, A., and Palmer, G., "Variable-Fidelity Euler-Lagrange Framework for Simulating Particle-Laden High-Speed Flows," *AIAA Journal*, Vol. 60, No. 5, 2022, pp. 3001–3019.

[16] Mirzaei, M., Shadaram, A., and Shahyar, M., "Numerical Simulation of Supersonic Gas-Particle Flow using Eulerian-Eulerian Approach," *14th AIAA/AHI Space Planes and Hypersonic Systems and Technology Conference*, 2006.

[17] Jung, S., and Myong, R., "A second-order positivity-preserving finite volume upwind scheme for air-mixed droplet flow in atmospheric icing," *Computers & Fluids*, Vol. 86, 2013, pp. 459–469. https://doi.org/https://doi.org/10.1016/j.compfluid.2013.08.001.

[18] Saurel, R., and Abgrall, R., "A Multiphase Godunov Method for Compressible Multifluid and Multiphase Flows," *Journal of Computational Physics*, Vol. 150, 1999, pp. 425–467.

[19] Loth, E., Daspit, J., Jeong, M., Nagata, T., and Nonomura, T., "Supersonic and Hypersonic Drag Coefficients for a Sphere," *AIAA Journal*, 2021, pp. 1–14.

[20] Fox, T., Rackett, C., and icholls, J., "Shock Wave Ignition of Magnesium Powders," *Proceedings of the 11th International Symposium on Shock Tubes and Shock Waves*, University of Washington Press, 1977.

[21] Steger, J. L., and Warming, R., "Flux vector splitting of the inviscid gasdynamic equations with application to finite-difference methods," *Journal of Computational Physics*, Vol. 40, No. 2, 1981, pp. 263–293. https://doi.org/https://doi.org/10.1016/0021-9991(81)90210-2.

[22] Mazaheri, A., Johnston, C., and Sefidbakht, S., "Three-Dimensional Radiation Ray-Tracing for Shock-Layer Radiative Heating Simulations," *Journal of Spacecraft and Rockets*, Vol. 50, No. 3, 2013, pp. 485–493.

[23] Johnston, C., and Mazaheri, A., "Impact of Non-Tangent-Slab Radiative Transport on Flowfield-Radiation Coupling," *Journal of Spacecraft and Rockets*, Vol. 55, No. 4, 2018, pp. 899–913.

[24] Dombrovsky, L., and Baillis, D., *Thermal Radiation in Disperse Systems: An Engineering Approach*, Begell House, Inc., 2010.

[25] Dyakonov2012, A., Schoenenberger, M., and Van Norma, J., "Hypersonic and Supersonic Static Aerodynamics of Mars Science Laboratory Entry Vehicle," *43rd AIAA Thermophysics Conference*, New Orleans, LA, 2012.

[26] West, T. K., and Johnston, C. O., "Assessment of Mars 2020 Forebody Heating Predictions with Coupled Material Response," *AIAA SciTech Forum*, National Harbor, MD, 2023.

[27] Zhao, W., Sun, Z., and Alwahabi, Z. T., "Emissivity and Absorption Function Measurements of Al2O3 and SiC Particles at Elevated Temperature for the Utilization in Concentrated Solar Receivers," *Solar Energy*, Vol. 207, 2020, pp. 183–191.

[28] West, T. K., Theisinger, J. E., Brune, A. J., and Johnston, C. O., "Backshell Radiative Heating on Human-Scale Mars Entry Vehicles," *AIAA Aviation*, Denver, CO, 2017.

[29] Johnston, C., West, T. K., and Brandis, A. M., "Features of Afterbody Radiative Heating for Titan Entry," *AIAA Aviation*, Dallas, TX, 2019.

[30] Lavvas, P., Yelle, R. V., and Griffith, C. A., "Titan's Vertical Aerosol Structure at the Huygens Landing Site: Constraints on Particle Size, Density, Charge, and Refractive Index," *Icarus*, Vol. 210, 2010, pp. 832–842.

[31] Ramsey, P., and Lyne, J. E., "Investigation of Titan Aerogravity Assist for Capture into Orbit About Saturn," *Journal of Spacecraft and Rockets*, Vol. 43, No. 1, 2006, pp. 231–233.

[32] Gnoffo, P., Gupta, R., and Shinn, J., "Conservation Equations and Physical Models for Hypersonic Air Flows in Thermal and Chemical Nonequilibrium," Tech. Rep. 19890006744, NASA, Feb. 1989.

[33] Thompson, K., Hollis, B., Johnston, C., Kleb, B., Lessard, V., and Mazaheri, A., "LAURA Users Manual 5.6," Tech. Rep. TM-2020-220566, NASA, 2020.